Structural determination and packing analysis of a cholesteryl caprate/cholesteryl laurate solid solution

Mary P. McCourt,* Phyllis Strong,† Walter Pangborn,† and Douglas L. Dorset[1,*]

Electron Diffraction Department, *Medical Foundation of Buffalo, Inc., 73 High Street, Buffalo, NY 14203; and Molecular Biophysics Department,† Medical Foundation of Buffalo, Inc., 73 High Street, Buffalo, NY 14203

Abstract This paper describes the X-ray crystal structure analysis of a cholesteryl ester solid solution, cholesteryl decanoate/cholesteryl laurate, grown from a bulk concentration with molar ratio 0.56/0.43. The unit cell is monoclinic with a = 12.969, b = 9.048, c = 31.137 Å, and β = 91.12° and the space group $P2_1$ with Z = 4 (two molecules per asymmetric unit). The cell constants closely represent an average value of crystal parameters for the two pure components (hence, nearly corresponding to Vegard's law). Although the overall monolayer 1 lamellar packing is superficially similar to the earlier-studied cholesteryl undecanoate/cholesteryl laurate solid solution, a more partitioned distribution of acyl chains, i.e., a microfractionation corresponding to the observed nonideal phase behavior, is suggested. The behavior is similar to that found for n-paraffin binaries cooled below a binodal phase boundary. Although it cannot be detected conclusively in this determination (due to high thermal motion of terminal acyl chain atoms), the non-stoichiometric combination of components also requires some partial occupancy of atomic sites on the chain termini. This structural arrangement is contrasted with the alternative expression found earlier for the more ideal undecanoate/laurate solid solution, i.e., random co-packing leading to fractional atomic occupancy in an average laurate structure. The final weighted R factor for 4578 reflections is 0.138.—**McCourt, M. P., P. Strong, W. Pangborn, and D. L. Dorset.** Structural determination and packing analysis of a cholesteryl caprate/cholesteryl laurate solid solution. *J. Lipid Res.* 1994. **35:** 584–591.

Supplementary key words X-ray crystallography • cholesteryl esters • binary phases

Atherosclerosis is currently one of the leading causes of death in the civilized world (1). To understand this disease, it is necessary to investigate the interactions among the various lipids involved in the formation of the arterial plaque, which causes the life-threatening ischemia. In a plaque, which consists of neutral and polar lipids, including cholesteryl esters, there is a layered concentration gradient of these polar and neutral components that can be represented by several points on a ternary phase diagram (2). This physical-chemical model seems to map the formative progress of the developing fatty lesion to a gruel plaque. It is clear, moreover, that bulk studies of these lesions can be misleading, since, in local aggregations of lipid, there are different melting points, which correspond to different individual populations of the fatty components (3). An overview of the lipid physical biochemistry involved in the progression and regression of atherosclerotic lesions has been given by Small (4).

Models of the progress of the fatty lesion have been based on the cosolubilities of the lipid components (2). Although these components (except for cholesterol in the final stages of plaque development) pack in the liquid crystalline state, crystal structures have been consulted to obtain some initial idea of the molecular conformations (5). As cholesteryl esters represent a major fraction of plaque lipid, the incorporation of various chain lengths into the arterial plaque requires the development of a more basic understanding on a molecular level of how these aggregations are stabilized, i.e., to judge how molecular volume differences may affect how these esters phase-separate and thus form immobilized lipid masses. Although it often has been the behavior of saturated chain derivatives that has been considered in many studies, chain unsaturation is also an important variable, as the major esters in plaque include only one saturated component (palmitate) while two others (oleate and linoleate) have acyl chains with double bonds. It is hoped, therefore, that a study of the binary solid state for the cholesteryl esters might provide some insights for modeling the binary or polydisperse liquid crystalline state and, indeed, was the impetus behind the first X-ray crystal structure determination of a cholesteryl ester solid solution (6).

The rules for the formation of binary solid solutions of saturated cholesteryl esters have been recently worked out after construction of phase diagrams for binary compositions of homologous compounds (7, 8). Electron diffraction measurements on these solids (7) support Kitaigorodskii's

Abbreviations: DSC, differential scanning colorimetry.

[1]To whom correspondence should be addressed.

statement (9) that, for cosolubility, two pure components should have the same or symmetrically compatible crystal structures. If near neighbors favor different layer packings, there will be fractionation, no matter how small the formal molecular volume difference is between the two similar structures (8). In the case of the cholesteryl esters that pack in the same crystal structure, the conditions for stability of solid solutions seem to resemble those for the n-paraffins (10, 11), even when the crystal packing does not include a sequestered methylene subcell component for the acyl chains.

With increasing difference in molecular volume between the components in a solid solution, it is clear that the melting behavior of these solid solutions deviates significantly from Raoult's law. In our first X-ray crystallographic study of these solid solutions (6), we found that a difference of one chain methylene unit is easily incorporated into the longer chain crystal structure and the only structural consequence of this average ester packing is a subtle shortening of some average intermolecular contact distances. When the chains differ by two methylene units, on the other hand, the phase behavior is expected to be less ideal (7, 8), perhaps leading to more salient differences in the average crystal structure. In order to investigate the possibility of new structural manifestations, the X-ray crystal structure of a nearly 1:1 molecular composition of cholesteryl caprate/cholesteryl laurate (see **Fig. 1** for numbering scheme) was carried out at room temperature. From this, it is possible to visualize the average layer packing that accounts for this nonideal phase behavior.

MATERIALS AND METHODS

Cholesteryl esters: crystal growth, thermal and electron diffraction measurements

Cholesteryl caprate and cholesteryl laurate, both stated to be 99+% pure, were purchased from Nu-Chek Prep Inc. (Elysian, MN). A combined sample at a molar ratio 0.56/0.43 was weighed into a small glass vial and this was then dissolved by warming in an excess of n-pentanol. The uncovered vial was left to evaporate for a month, whereupon lath-like crystals were formed (major crystal face (001) and elongated along [010]). Other molar combinations were weighed into aluminum DSC pans which were then sealed for determination of the phase diagram from the endothermic peaks (7, 8). These thermal measurements were made with a Mettler TA-3300 instrument, in which the melting temperature range was calibrated by a polynomial fit to the melting peaks of indium, lead, and zinc, and the transition enthalpies against the value for pure indium. Typical heating scans for several binary combinations are represented in **Fig. 2.** For solids rich in caprate, both the crystal-to-smectic and smectic-to-melt transitions are observed when the samples are heated. All samples cooled from the melt will exhibit both isotropic-to-cholesteric and cholesteric-to-smectic transitions (see Fig. 3). These observations are consistent with those made for the pure components (12). After the DSC measurements were completed, samples were scraped out of the re-opened DSC pans and dissolved in amyl alcohol. As described earlier (7), these were then evaporated onto a mica sheet and then epitaxially recrystallized on benzoic acid. Selected area electron diffraction patterns were then obtained at 100 kV with a JEOL JEM-100CXII electron microscope. Lattice spacings were calibrated with an internal gold powder diffraction standard.

X-ray diffraction

After determination of approximate unit cell constants from film measurements with a precession camera, the crystal was mounted on the goniometer of an Enraf-Nonius CAD-4 X-ray diffractometer. Intensity data were collected using Ni-filtered CuKα radiation after refinement of the cell constants by least squares fit to 25 reflections. Periodically, standard reflections were monitored to detect the occurrence of radiation damage to the crystal. In all, 9116 unique reflections were measured, of which 5038 were judged to be unobserved, based on the criterion that $IF_oI < 3.0\ \sigma IF_cI$. The cell dimensions of the approximately 1:1 mole fraction caprate/laurate mixture are intermediate between those of the individual pure compo-

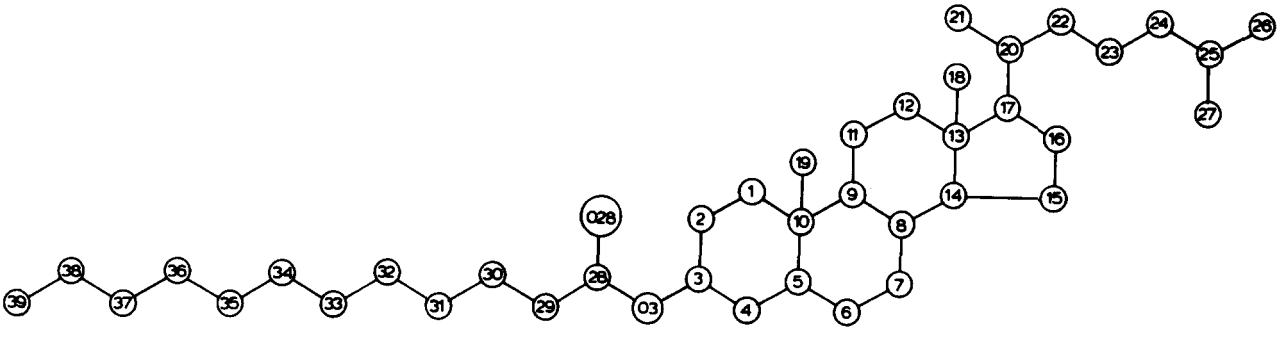

Fig. 1. Numbering scheme for the cholesteryl ester (cholesteryl laurate represented). Oxygens are labeled O3 for the carbonyl, O28 for the linkage to the chain. All other atoms are carbon. Hydrogens are not represented.

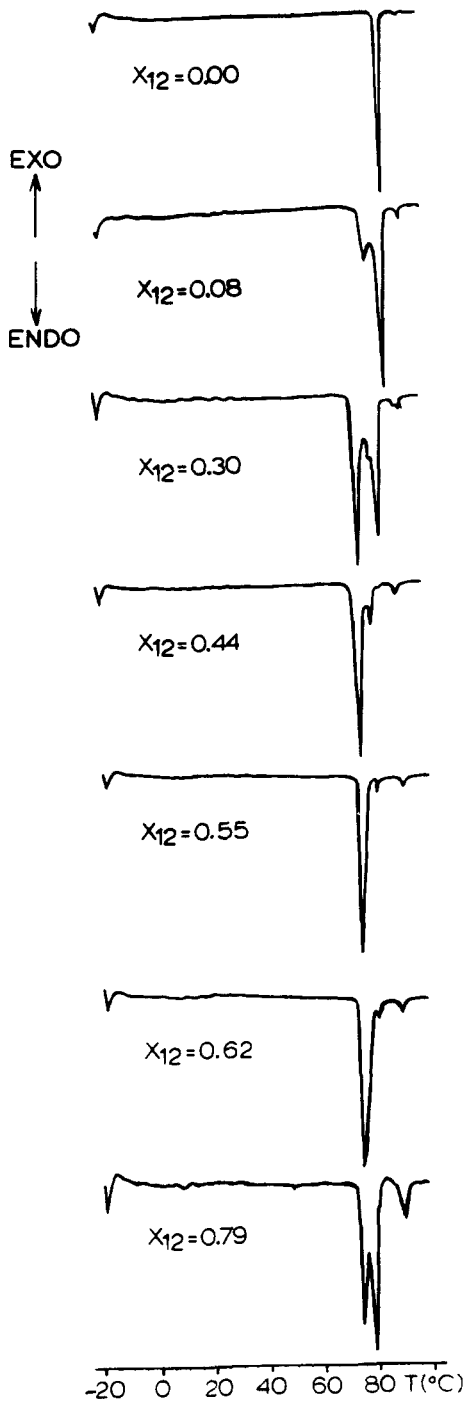

Fig. 2. Representative DSC heating scans for cholesteryl ester combinations. Peak temperatures from the main endothermic positions are plotted in Fig. 3. Samples rich in the laurate ($X_{12} > 0.79$) undergo a kinetic recrystallization (exotherm) phenomenon if the scan rate is too fast (e.g., 5 deg/min) but this disappears when the heating rate is slower (e.g., 2 deg/min). Plots of the phase diagram were made using scans without this non-equilibrium event.

nents of caprate and laurate at room temperature (**Table 1**). The space group for the solid solution of caprate and laurate as well as the individual pure components (5) is noncentrosymmetric, i.e., $P2_1$, as revealed by systematic absences in the 0k0 reflections.

Structure analysis

The data were processed using the series of programs of Blessing (13) with a modified weighting scheme. For initial phasing of the structure factor magnitudes, a trial model based on a previous determination of the undecanoate/laurate structure (6) was used with the numbering scheme for the cholesteryl ester molecules shown in Fig. 1. In the initial model, only the cholesteryl nuclei were included and refined isotopically. Subsequent Fourier difference maps located atomic positions for other heavy atoms in the structure. All 80 atoms were eventually included in the full least squares refinement with 64 atoms being refined anisotropically. This resulted in a structure where the laurate and caprate molecules seemed to be uniquely defined with no partial occupancy identified conclusively for either molecular chain. As done in the earlier determination (6), efforts were made to locate partial (e.g., 50%) occupancy positions for two additional terminal carbon atoms of the decanoate. Also partial positions were tested for the two terminal positions of the laurate chain. However, attempts to refine these sites resulted in a disrupted bonding geometry in these regions of the structure. The attempt is frustrated further by the high temperature parameters for the terminal chain atoms. Other attempts to locate density in this region included the calculation of a $2IF_oI-IF_cI$ map that did not reveal any additional or lower peak positions. Nevertheless, the non-stoichiometric combination of components requires partial occupancy of some chain sites, especially since the phase diagram (see Fig. 3) does not indicate the presence of a strict 1:1 molecular compound.

Difficulties in structure refinement were experienced in several regions of the two molecules. After location of atomic positions, the isoprenoid chain of the laurate component had to be held fixed; otherwise refinement of this local geometry led to chemically meaningless results. Positional disorder is manifested by the rather high isotropic thermal parameters, B = 30 Å^2 for C24 and B = 40 Å^2 for C25, C26, and C27. The C39 atom of the laurate structure was also difficult to refine; after isotropic refinement, it had a final B value of 46 Å^2, in contrast to the equivalent value of the earlier investigated undecano-

TABLE 1. Unit cell dimensions

Parameter	Solid Solution	Cholesteryl Caprate (23)	Cholesteryl Laurate (22)
a, Å	12.969	12.931	12.989
b, Å	9.048	9.066	9.008
c, Å	31.137	30.220	32.020
β, °	91.120	91.140	91.360

ate/laurate structure C39, B = 19 Å^2. The refinement was restarted several times with a corrected geometry for this position, but it ended up consistently with an enlarged bond length to C38. The caprate ester refines to lower B values than the laurate in the isoprenoid end, i.e., for C25, C26, and C27, these are respectively 20, 26, and 23 Å^2. These compare to 16, 20, and 20 Å^2 for the respective equivalent atoms in the undecanoate/laurate determination (6). The acyl chain termini of the caprate also refines to somewhat lower B values (C36 and C37: 30 and 34 Å^2, respectively) than the terminal atoms of the laurate. After the heavier atom positions were located, hydrogens were added at appropriate positions with theoretical bond distances and angles. The final R factor for all atoms refined against 4578 reflections (rejecting 8 low angle measurements on the basis of a normal probability distribution plot (14)) is 0.138. The unweighted R, including all unobserved reflections, is 0.124.

RESULTS

The experimental phase diagram for binary combinations of cholesteryl caprate with cholesteryl laurate (**Fig. 3**) resembles one already published for cholesteryl nonanoate/undecanoate binary compositions (8), including the positions of concentration-dependent mesomorphic transitions measured from binary samples cooled from the melt. That is to say, the two molecules are continuously co-soluble over all concentrations (as verified by electron diffraction measurements of lamellar spacing for the epitaxially oriented samples over the concentration range). However, the melting point curve deviates markedly from the ideal one calculated from Raoult's law, using relations derived by Lee (15). The phase behavior, therefore, is distinct from the nearly ideal co-solubility found for the cholesteryl undecanoate/laurate binaries (8). As found also in the cholesteryl undeconoate/cholesteryl laurate binary phase diagram (7), there are two isothermal transition lines below the major phase change temperature. Do these correspond to a eutectic relationship? A theoretical eutectic temperature, T = 67.5°C for the cholesteryl caprate/cholesteryl laurate, is well below the isotherm temperature in Fig. 3. This calculation, using ΔH values (major endotherm) for the pure components, correctly predicts this phase separation behavior in cholesteryl esters when it occurs (8), and thus, we find that these measured isotherms do not represent a solidus line for an eutectic solid, again indicating that the two components are co-soluble over all concentrations. In further support of this co-solubility, electron diffraction patterns of the binary solids only indicate the monolayer I structure with a nearly linear increase of lamellar spacings with increasing concentration of the longer component, as was also the case for the cholesteryl undeconoate/cholesteryl laurate binaries (7). Because cholesteryl laurate is polymorphic, as found originally by Sawzik and Craven (16), this co-solubility is an important observation. The second polymorphic form of the ester was identified earlier (7) by electron diffraction experiments to be the bilayer packing, not the monolayer II form proposed earlier (16) from powder X-ray measurements. When the laurate is combined with myristate (7), for example, the minor bilayer polymorph is expressed, in addition to the monolayer I structure, and is readily observed in electron diffraction experiments. However, when it is combined with pure esters that pack only in the monolayer I structure, the second polymorph is not found. Hence we do not expect the bilayer polymorph to be a contaminant of our larger crystals grown for X-ray data collection.

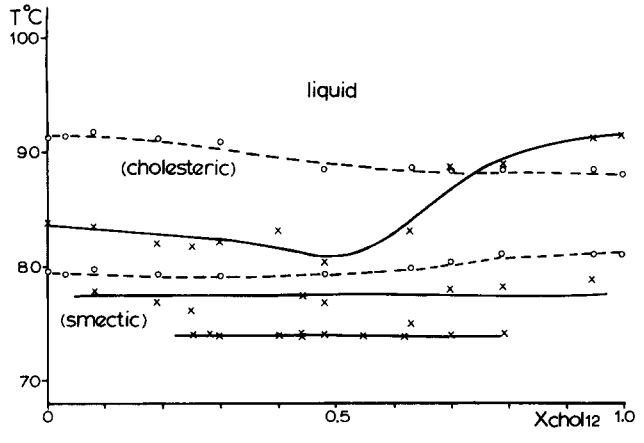

Fig. 3. Binary phase diagram for the cholesteryl ester solid solution, cholesteryl caprate/cholesteryl laurate. The points "x" are peak temperatures from the above plots from crystal-crystal-, or crystal-disordered phase-, transitions. (Liquid crystalline transitions, which are continuous with concentration, are seen in cooling samples from the melt, and are indicated by dashed lines with experimental points marked by "o".) Isothermal crystal crystal transitions (also observed in the phase diagrams of cholesteryl caprate/cholesteryl undeconoate and cholesteryl laurate/cholesteryl myristate (7, 8)) would possibly suggest conversions from one polymorph to another but electron diffraction spacings at room temperature reveal that the solid packs only in the monolayer I structure at all concentrations.

The appearance of the phase diagram in Fig. 3 is also very similar to the ones found for the n-paraffin binaries where the molecular volume differences cause a similar deviation from Raoult's law behavior. That is to say, the main transition endothermic temperature has a minimum near the midpoint of the concentration range (17). This, however, implies nothing about the structure of the binary solid solutions as shown in subsequent electron diffraction studies (18, 19). For example, it does not necessarily imply the existence of a 1:1 molecular complex. On the other hand, the binary phase behavior of the major transition line may indeed imply the existence of a miscibility gap at lower temperature (20), as will be discussed further below. Our structural studies of similar paraffin binaries (21), moreover, anticipate a solid with some partial fractionation of molecular components.

In keeping with these observations, the molecular packing of the caprate and laurate in the X-ray crystal structure determination (**Fig. 4**) has the same monolayer I arrangement (5) found for the undecanoate/laurate structure (6) or for pure esters with acyl chains less than 14 carbons but greater than 8 carbons in length. The molecular conformations of the molecules are also consistent with previous determinations for the pure components (22, 23). For example, the conformation of the acyl chain of the longer molecule corresponds to the Sawzik and Craven (22) room temperature determination of the cholesteryl laurate. **Table 2** lists the torsion angles of the laurate/caprate solid solution as well as the values for caprate (23) and laurate (22). Both acyl chains are fully extended, but the high thermal parameters point to the possibility of conformational disorder. The acyl chains of the two molecules in the asymmetric unit are in different environments, again consistent with previous determinations. A listing of all atoms and their thermal parameters is shown in **Table 3.** Bond distances are listed in **Table 4.** Note that the inaccuracy of these lengths is also observed in the pure component crystal structures solved at room temperature (22, 23), particularly for the acyl chain parameters. Torsion angles are in Table 2 and nearest neighbor contacts can be found in **Table 5.**

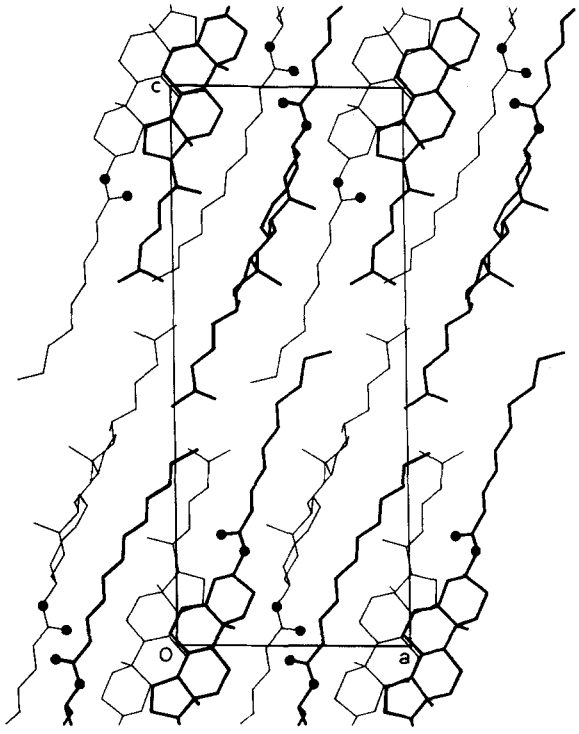

Fig. 4. Unit cell of solid solution of cholesteryl caprate/cholesteryl laurate solid solution showing details of the average molecular packing in the monolayer I form.

TABLE 2. Torsion angles for isoprene and acyl terminal chain atoms (°)

			Pure Esters			
	Solid Solution		Caprate		Laurate	
Torsion Angle	Caprate	Laurate	A	B	A	B
22-23-24-25	−170.2	−167.1	−41	178	−174	162
23-24-25-26	175.3	60.0	168	−57	−171	−40
23-24-25-27	−78.6	−170.0	−81	152	37	165
28-29-30-31	179.3	−175.3	−176	−174	−170	171
29-30-31-32	−177.8	177.0	179	−175	175	−170
30-31-32-33	−176.6	−174.0	−176	−175	−179	−177
31-32-33-34	177.0	172.5	167	162	174	175
32-33-34-35	−160.6	−170.1	−170	164	−167	−178
33-34-35-36	−168.8	179.6	179	90	177	159
34-35-36-37	−167.7	179.3	−171	174	171	−161
35-36-37-38		176.3			171	179
36-37-38-39		174.9			170	−171

DISCUSSION

Given the previous experience with the undecanoate/laurate solid solution crystal packing, the structural determination for the caprate/laurate binary has led to a result which, initially, was somewhat surprising. Based on the earlier determination, as well as the crystal structure analysis of a paraffin solid solution (19), the molecular species were expected to be intimately co-mixed, so that the co-solubility of these would be expressed mainly by a fractional occupancy of outer atomic sites on the acyl chains. However, this is not what is observed for this structure. Although the phase diagram in Fig. 3 and the continuity of electron diffraction lamellar spacings do indicate that the two components initially are continuously co-soluble over all concentrations in a monolayer I packing scheme when crystallized from the melt, the crystal structure reveals the beginning of a microfractionation process. Although the crystal structure probably is not a strict 1:1 binary combination of components, the fractionation could involve the formation of lateral microdomains, leading to the average structure seen in this X-ray determination. This would be somewhat similar to the fractionation process observed for metastable paraffin solutions held below the miscibility gap (e.g., at room temperature), in which a gradual separation of solid solutions is found to occur (21). Vibrational spectroscopic measurements using deuterated compounds as labels indicate that small islands of laterally ordered domains appear in time (24), in addition to the electron diffraction measurement (21) of a superlattice-like repeat of the lamellar spacing, indicating growth of an incommensurate phase. Such a structure is also found to persist for the eutectic interaction of paraffin solid solutions occurring when the volume difference increases. The phase separa-

TABLE 3. Fractional coordinates and B values for non-hydrogen positions

	Molecule 1				Molecule 2			
	x	y	z	Biso	x	y	z	Biso
C1	−0.482583	0.227943	0.161670	9.25	0.718929	0.097445	0.951044	8.29
C2	−0.542807	0.183937	0.121499	9.24	0.669309	0.070893	0.905252	9.44
C3	−0.515344	0.027186	0.108598	7.75	0.760522	0.080479	0.873902	9.03
C4	−0.541147	−0.081873	0.142905	9.45	0.839418	−0.039840	0.882036	8.97
C5	−0.489350	−0.036892	0.185195	8.03	0.882065	−0.026561	0.928850	7.27
C6	−0.437115	−0.139633	0.207203	10.08	0.981515	−0.023280	0.935244	7.91
C7	−0.382269	−0.111735	0.250155	10.35	1.034817	−0.015315	0.979571	7.74
C8	−0.412859	0.034249	0.270187	9.46	0.957309	−0.038570	1.015713	6.93
C9	−0.420436	0.157402	0.236522	7.88	0.856809	0.039567	1.005958	6.91
C10	−0.501715	0.117987	0.200756	8.50	0.802621	−0.018335	0.964209	7.30
C11	−0.437707	0.312699	0.257287	11.71	0.781422	0.035642	1.043947	8.77
C12	−0.361156	0.351325	0.293201	11.97	0.834856	0.088608	1.087149	8.95
C13	−0.356269	0.224712	0.328780	11.29	0.934608	0.003163	1.096301	7.21
C14	−0.331870	0.077504	0.305432	10.35	1.002745	0.019357	1.057308	7.17
C15	−0.310322	−0.032572	0.340265	12.92	1.109926	−0.042088	1.074881	8.23
C16	−0.255613	0.063007	0.376784	16.51	1.116369	0.011804	1.121077	9.51
C17	−0.266026	0.231356	0.359918	13.18	1.005704	0.069519	1.131910	7.87
C18	−0.457716	0.220873	0.354091	14.54	0.913402	−0.162038	1.107495	9.76
C19	−0.616030	0.137623	0.217666	10.02	0.753158	−0.172331	0.969693	8.74
C20	−0.270875	0.341715	0.399580	15.93	0.982337	0.037908	1.180808	9.04
C21	−0.281546	0.514101	0.382008	19.06	0.871972	0.086765	1.192033	10.77
C22	−0.167576	0.318578	0.423955	19.78	1.057328	0.128115	1.208575	11.51
C23	−0.171519	0.372524	0.469424	28.29	1.054985	0.084975	1.256648	14.84
C24	−0.072867	0.335322	0.499967	30.00	1.138129	0.184811	1.283522	16.34
C25	−0.086080	0.358630	0.545280	40.00	1.145424	0.118094	1.328740	20.03
C26	−0.175250	0.259290	0.560860	40.00	1.236446	0.217749	1.350176	26.11
C27	0.014190	0.348230	0.573030	40.00	1.044168	0.179863	1.351711	23.68
C28	−0.552534	0.030481	0.032424	9.22	0.731429	0.132417	0.797777	11.31
C29	−0.622087	−0.033337	−0.003256	9.00	0.675271	0.093048	0.758365	11.69
C30	−0.608512	0.041177	−0.045018	8.71	0.679525	0.206829	0.723798	13.11
C31	−0.685406	−0.017110	−0.078740	8.94	0.618852	0.153073	0.683541	15.55
C32	−0.680425	0.057489	−0.120944	8.67	0.624925	0.260521	0.648132	17.89
C33	−0.768296	0.005430	−0.153008	10.56	0.560133	0.213724	0.608874	18.80
C34	−0.776181	0.091363	−0.194734	10.50	0.564445	0.321142	0.565312	30.10
C35	−0.873302	0.054999	−0.221267	13.30	0.458254	0.281955	0.534012	23.90
C36	−0.876626	0.147222	−0.263055	14.81	0.437562	0.336077	0.484854	30.03
C37	−0.976508	0.097140	−0.286050	21.29	0.323142	0.305815	0.472056	34.28
C38	−0.979911	0.197501	−0.324935	32.33				
C39	−1.097759	0.105306	−0.349909	46.91				
O3	−0.579208	−0.020494	0.071349	9.38	0.709954	0.053089	0.831123	10.58
O28	−0.481031	0.114931	0.027440	10.71	0.801949	0.220967	0.081932	21.10

TABLE 4. Bond lengths of isoprene and acyl chain terminal atoms Å

	Solid Solution	
	Molecule A (Caprate)	Molecule B (Laurate)
C24-C25	1.533	1.440
C25-C26	1.619	1.550
C25-C27	1.608	1.550
C28-C29	1.459	1.530
C28-O3B	1.297	1.348
C28-O28	1.221	1.214
C29-C30	1.491	1.478
C30-C31	1.545	1.528
C31-C32	1.473	1.480
C32-C33	1.530	1.573
C33-C34	1.670	1.516
C34-C35	1.709	1.529
C35-C36	1.624	1.546
C36-C37	1.553	1.536
C37-C38		1.513
C38-C39		1.895

tion of cholesteryl esters below the miscibility gap boundary seems to use only the lateral mechanism for molecular aggregation. Its onset also seems to be more sensitive to volume differences between the two species than for the n-paraffins. For example, the Kitaigorodskii (9) overlap parameter ϵ is 0.94 for these esters compared to 0.83 for the onset of phase separation in the normal alkanes (11). The difference is probably due to the inability for esters to translate along their long axes in mixed component layers, a disorder mechanism that is important, however, for paraffin binaries (19). Given this non-ideal nature of the binary interaction between these two components, it is also clear that the observed micro-fractionation phenomenon is the easiest way to cope with the increased difference in molecular volume found in the 10/12 pair, whereas the slighter volume difference of the 11/12 pair can be more easily compensated by a local co-mixing of

TABLE 5. Nearest neighbor contacts Å

	Solid Solution[a]	
	10/12	11/12
Molecular interactions between the average caprate molecules		
C33-C37 (C38*)	4.44	3.86
C34-C37 (C38*)	4.83	4.31
C35-C37 (C38*)	4.85	4.31
C37-C37 (C38*)	6.32	5.90
C38-C38*		6.88
C25-C37 (C38*)	5.25	5.97
C26-C37 (C38*)	4.00	3.86
C27-C37 (C38*)	5.08	5.89
Molecular interactions between average caprate and laurate molecular species		
C25-C39	4.85	4.98
C25-C25	5.19	5.15
Molecular interactions between average laurate molecules		
C25-C39	4.26	4.32
C25-C25	5.60	5.35

[a]Indicated interactions for 10/12 are compared to 11/12 structure for molecules at equivalent sites in the layers; *indicates partial atomic occupancy position in 11/12 pair.

acyl chains (also expressed by the nearly ideal nature of its phase diagram).

Although the layer packings for the respective 10/12 and 11/12 structures are virtually indistinguishable from each other (**Fig. 5**), there are two regions where salient differences do exist in addition to the nascent sequestering of the pure chains in the former. These regions are where the isoprene tail of the average caprate molecule interacts with the acyl end of the average laurate molecule. The slight differences at the isoprene tails are what might be expected from the observed large B values, indicating thermal or positional disorder. At another site, the 10/12 and 11/12 structures have different acyl chain conformations that allow the 10/12 structure to maintain contacts to the isoprene tails of the adjacent molecules similar to those for the 11/12 structure (Fig. 5). The contact distance at this junction for C39–C25 of the 11/12 structure is 3.6 Å, while the C37–C25 contact is 4.0 Å for the 10/12 structure.

Obviously, some features of this molecular co-packing remain unclear, so that a precise description of local fractional atomic occupancies cannot be made. It is clear that low temperature structure determinations would be very beneficial for both 11/12 and 10/12 binaries for clearer resolution of atomic loci as their thermal motion is reduced. (A similar comparison has already been reported for the pure laurate structure, for example (16), as well as some unsaturated chain esters (25–27).) However, such work must be carried out with the realization that the lower crystal density can also induce local changes in crystal packing (e.g., the induction of an end-*gauche* conformation in the pure laurate structure). Indeed, both the completed and proposed studies at room and low temperatures are equally important, the former for giving an overall picture of the crystal packing nearer to physiological conditions and the latter for a better specific visualization of atomic placement in a long chain solid solution.

This research was supported in part by the Helen Woodward Rivas Memorial Trust.

Manuscript received 3 March 1993, in revised form 7 July 1993, and in re-revised form 18 October 1993.

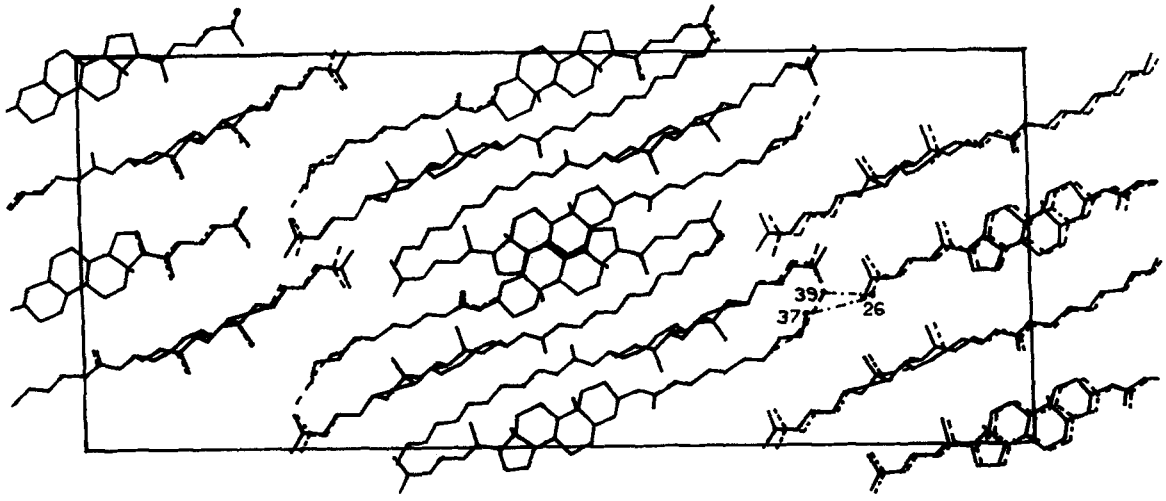

Fig. 5. Unit cell superposition of cholesteryl caprate/cholesteryl laurate with cholesteryl undecanoate/cholesteryl laurate. Despite differences in the layer packings for the two solid solutions, contact distances between molecules are very similar (see Table 5). For example, the distance between the C39-C26 (11/12 structure) is 3.96 Å and the distance between the C37-C26 (10/12 structure) is 4.0 Å. The unit cell sizes are virtually identical for the two solid solutions.

REFERENCES

1. Brown, M. S., and J. L. Goldstein. 1983. Lipoprotein metabolism in the macrophage: implications for cholesterol deposition in atherosclerosis. *Annu. Rev. Biochem.* **52:** 223–261.
2. Small, D. M., and G. G. Shipley. 1974. Physical-chemical basis of lipid deposition in atherosclerosis. *Science.* **185:** 222–229.
3. Katz, S. S., D. M. Small, F. R. Smith, R. B. Dell, and D. S. Goodman. 1982. Cholesterol turnover in lipid phases of human atherosclerotic plaque. *J. Lipid Res.* **23:** 733–737.
4. Small, D. M. 1988. Progression and regression of atherosclerotic lesions. Insights from lipid physical biochemistry. *Atherosclerosis.* **8:** 103–129.
5. Craven, B. M. 1986. Cholesterol crystal structures: adducts and esters. *In* Handbook of Lipid Research. Vol. 4. D. M. Small, editor. Plenum, New York. 149–152.
6. Dorset, D. L., and W. A. Pangborn. 1992. Molecular interactions in binary solids: crystal structure of a cholesteryl ester solid solution. *Proc. Natl. Acad. Sci. USA.* **89:** 1822–1826.
7. Dorset, D. L. 1987. Cholesteryl esters of saturated fatty acids: co-solubility and fractionation of binary mixtures. *J. Lipid Res.* **28:** 993–1005.
8. Dorset, D. L. 1988. Co-solubility of saturated cholesteryl esters: a comparison of calculated and experimental binary phase diagrams. *Biochim. Biophys. Acta.* **963:** 88–97.
9. Kitaigorodskii, A. I. 1961. Organic Chemical Crystallography. Consultants Bureau, New York. 231–240.
10. Dorset, D. L. 1990. Chain length and the cosolubility of n-paraffins in the solid state. *Macromolecules.* **23:** 623–633.
11. Dorset, D. L. 1993. Symmetry and the stability of binary solid solutions of linear molecules. *Acta Chim. Hung.* **130:** 389–404.
12. Ginsberg, G. S., D. Atkinson, and D. M. Small. 1984. Physical properties of cholesteryl esters. *Prog. Lipid Res.* **23:** 135–167.
13. Blessing, R. 1989. DREADD—data reduction and error analysis for single crystal diffractometer data. *J. Appl. Crystallogr.* **22:** 396–398 and references cited therein.
14. Howell, P. L., and G. D. Smith. 1991. Identification of heavy atom derivatives by normal probability methods. *J. Appl. Crystallogr.* **25:** 81–86.
15. Lee, A. G. 1977. Lipid phase transitions and phase diagrams. II. Mixtures involving lipids. *Biochim. Biophys. Acta.* **472:** 285–344.
16. Sawzik, P., and B. M. Craven. 1980. The structure of cholesteryl oleate at 198 K. *Acta Crystallogr.* **B36:** 3027–3033.
17. Dorset, D. L. 1985. Crystal structure of n-paraffin solid solutions: an electron diffraction study. *Macromolecules.* **18:** 2158–2163.
18. Dorset, D. L. 1987. Role of symmetry in the formation of n-paraffin solid solutions. *Macromolecules.* **20:** 2782–2788.
19. Dorset, D. L. 1990. Direct structure analysis of a paraffin solid solution. *Proc. Natl. Acad. Sci. USA.* **87:** 8541–8544.
20. Gordon, P. 1968. Principles of Phase Diagrams in Materials Systems. McGraw-Hill, NY. 82–105.
21. Dorset, D. L. 1990. Chain length and the co-solubility of n-paraffins in the solid state. *Macromolecules.* **23:** 623–633.
22. Sawzik, P., and B. M. Craven. 1979. The crystal structure of cholesteryl laurate at 298 K. *Acta Crystallogr.* **B35:** 789–791.
23. Pattabhi, V., and B. M. Craven. 1979. Crystal structure of cholesteryl decanoate. *J. Lipid Res.* **20:** 753–759.
24. Snyder, R. G., M. C. Goh, V. J. P. Srivatsavoy, H. L. Strauss, and D. L. Dorset. 1992. Measurement of the growth kinetics of microdomains in binary n-alkane solutions by infrared spectroscopy. *J. Phys. Chem.* **96:** 10008–10019.
25. Craven, B. M., and P. Sawzik. 1983. Conformation and packing of unsaturated chains in cholesteryl linolelaidate at 123 K. *J. Lipid Res.* **24:** 784–789.
26. Craven, B. M., and P. Sawzik. 1984. Conformational changes of cholesteryl palmitoleate in the crystal structure at low temperature. *J. Lipid Res.* **25:** 857–864.
27. Gao, Q., and B. M. Craven. 1986. Conformation of the oleate chains in crystals of cholesteryl oleate at 123 K. *J. Lipid Res.* **27:** 1214–1221.